Electronic Supplementary Information

A Small Library of Copper-Based Metallenes with Superior Antibacterial Activity

Zhaohua Miao,[‡a] Chenxin Lu,[‡a] Cheng-Yan Xu,[b] Yan Ma,[c] Zhong Cao,[de] Lulu Liu,[a] Deyan Gong,[a] and Zhengbao Zha[*a]

a. School of Food and Biological Engineering, Hefei University of Technology; Hefei 230009, China.

b. School of Materials Science and Engineering, Harbin Institute of Technology (Shenzhen), Shenzhen 518055, China.

c. School of Biomedical Engineering, Anhui Medical University, Hefei 230032, China.

d. School of Biomedical Engineering, Shenzhen Campus of Sun Yat-sen University, Shenzhen, Guangdong, 518107, China.

e. Shenzhen International Institute for Biomedical Research, Longhua District, Shenzhen 518116, Guangdong, China.

‡ These authors contributed equally: Zhaohua Miao, Chenxin Lu

** Corresponding author. E-mail: zbzha@hfut.edu.cn*

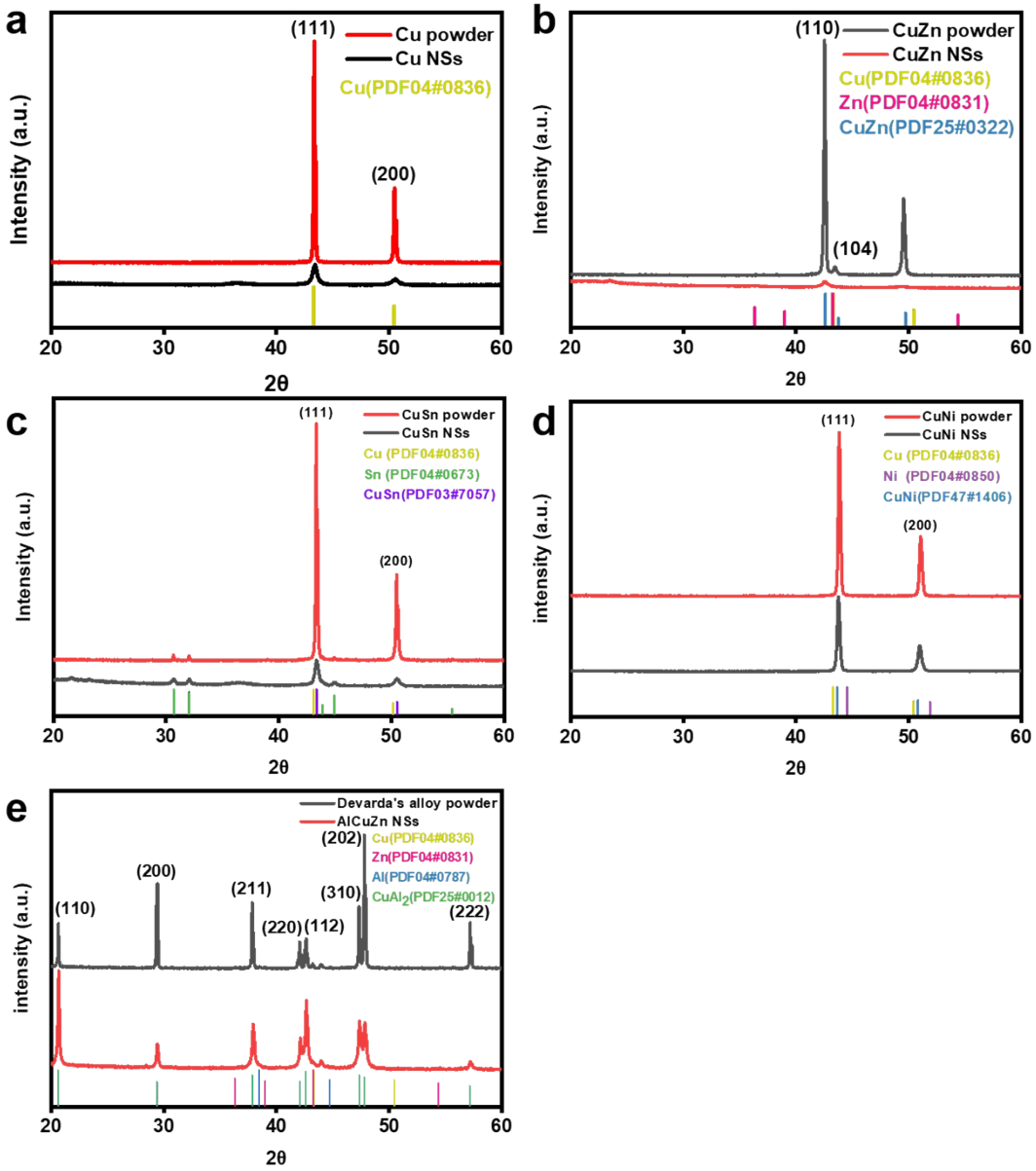

Fig. S1 XRD patterns of copper-based metallenes. (a) XRD patterns of Cu powder and Cu NSs. (b) XRD patterns of CuZn powder and CuZn NSs. (c) XRD patterns of CuSn powder and CuSn NSs. (d) XRD patterns of CuNi powder and CuNi NSs. (e) XRD patterns of Devarda's alloy powder and AlCuZn NSs.

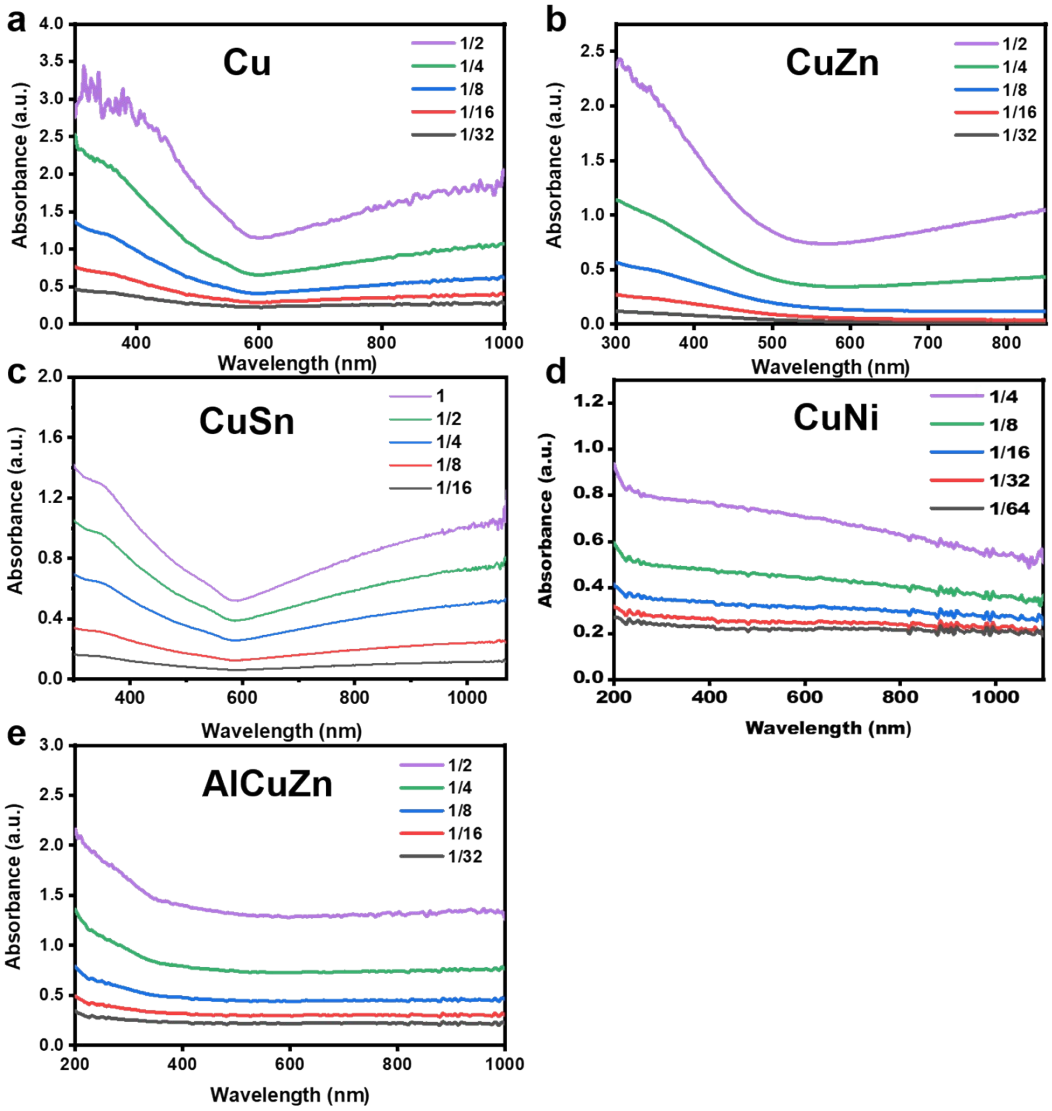

Fig. S2 UV–vis-NIR spectra of copper-based metallenes. UV–vis-NIR spectra of (a) Cu NSs, (b) CuZn NSs, (c) CuSn NSs, (d) CuNi NSs and (e) AlCuZn NSs at varying degrees of dilution.

Fig. S3 Dispersion images of copper-based metallenes. Photographs of copper-based metallene dispersions with /without laser.

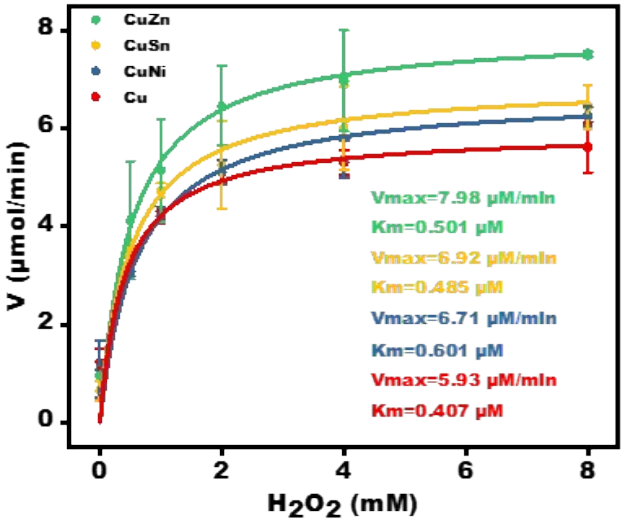

Fig. S4 Michaelis−Menten curve for H_2O_2.

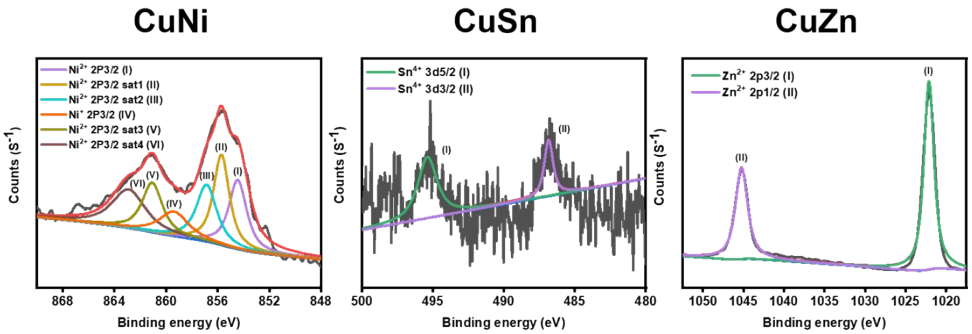

Fig. S5 XPS spectra of copper-based metallenes. 2p3/2 orbital for other elemental valence curves in Cu-based metallenes.

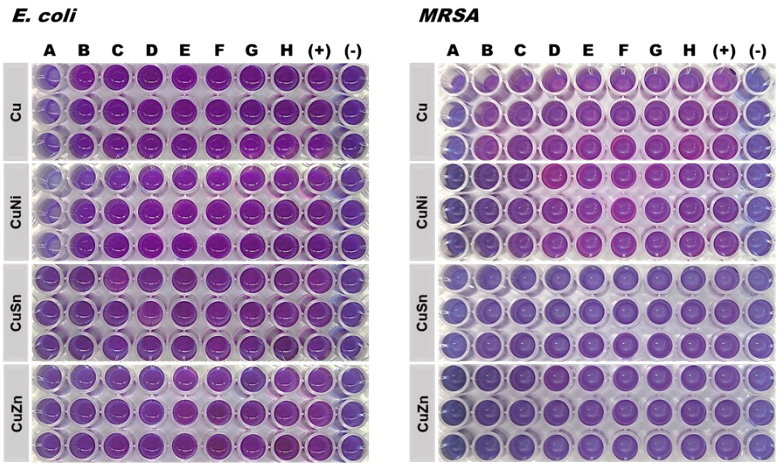

Fig. S6 The minimal inhibition concentrations of copper-based metallenes on MRSA (A: 4 μg/mL, B: 2 μg/mL, C: 1 μg/mL, D: 0.5 μg/mL, E: 0.25 μg/mL, F: 0.125 μg/mL, G: 0.0625 μg/mL, H: 0.03125 μg/mL).

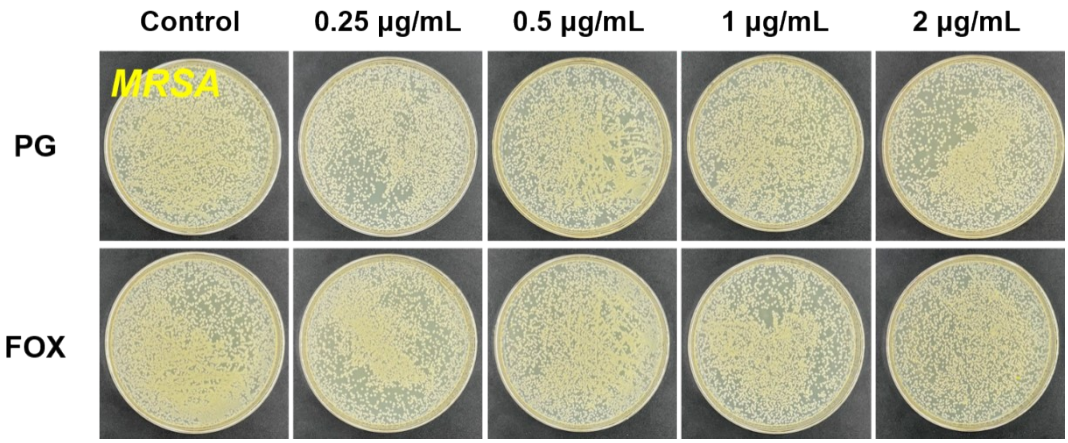

Fig. S7 Photographs of *MRSA* treated with PG and FOX *in vitro*. Photographs of bacterial colonies of *MRSA* after different treatments.

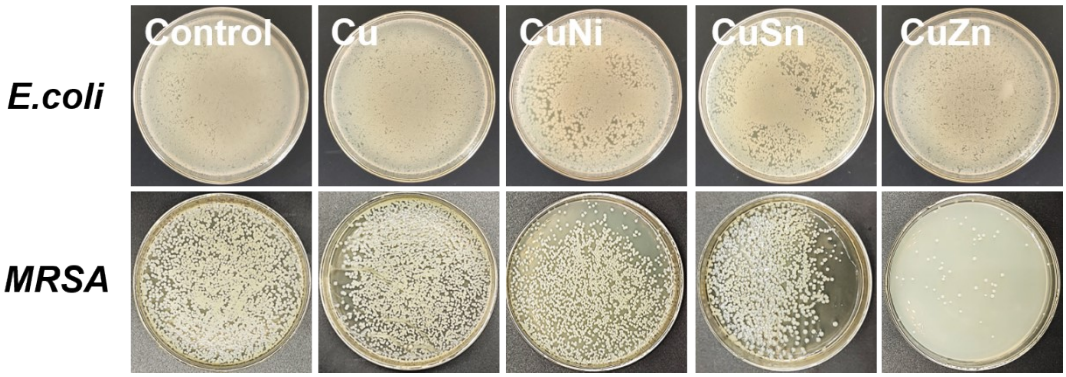

Fig. S8 Photographs of *E. coli* and *MRSA* treated with different copper-based raw powders.

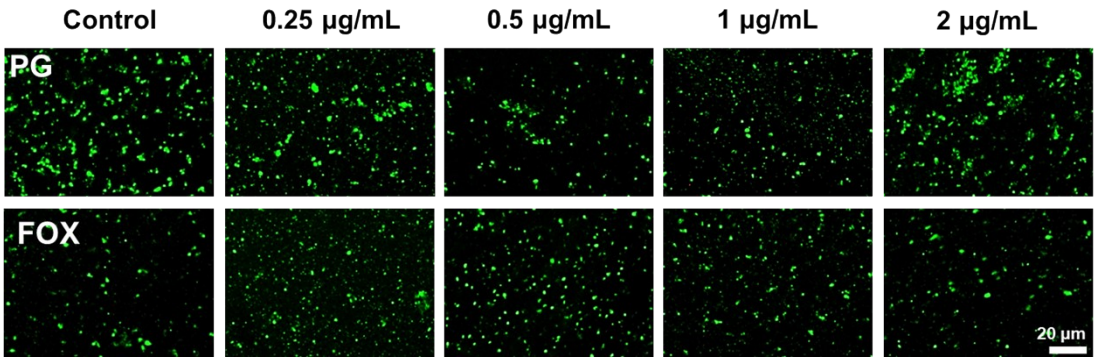

Fig. S9 Fluorescence staining images of *MRSA* using SYTO 9/PI probe after different antibiotic treatments.

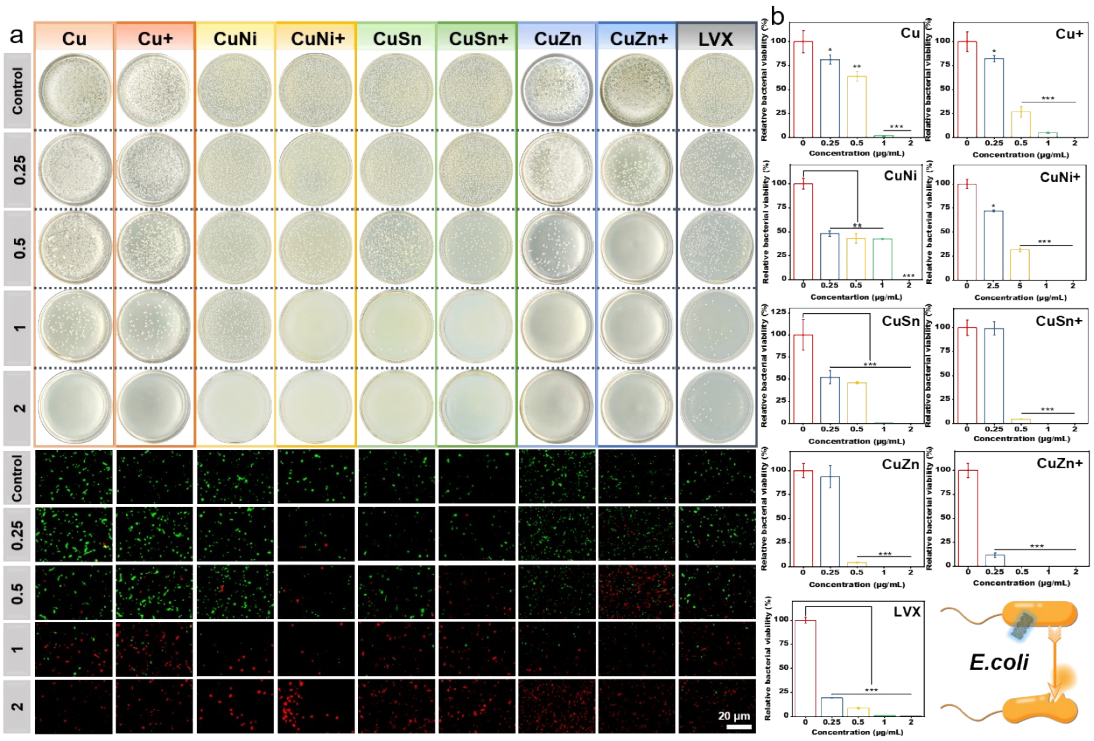

Fig. S10 Photographs and viability of *E. coli* treated with copper-based metallenes *in vitro*. (a) Photographs of bacterial colonies of *E. coli* after different treatments. (b) Relative bacterial viability of *E. coli* after treatment based on (a) (n = 3). (c) Fluorescence staining images of *E. coli* using SYTO 9/PI probes after different treatments (+ means plus H_2O_2, Concentration unit: μg/mL). One-way ANOVA was used to analyze multiple groups. (*p < 0.05, **p < 0.01, ***p < 0.001, and ****p < 0.0001)

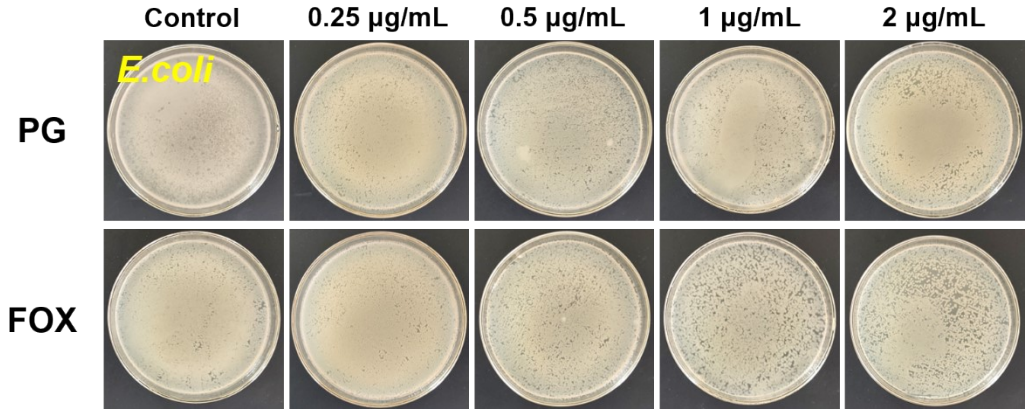

Fig. S11 Photographs of *E. coli* treated with PG and FOX *in vitro*. Photographs of bacterial colonies of *E. coli* after different treatments.

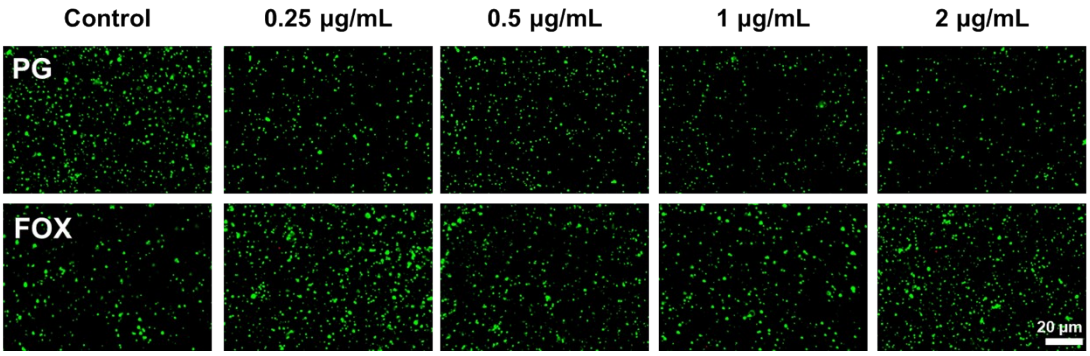

Fig. S12 Fluorescence staining images of *E. coli* using SYTO 9/PI probes after different antibiotic treatments.

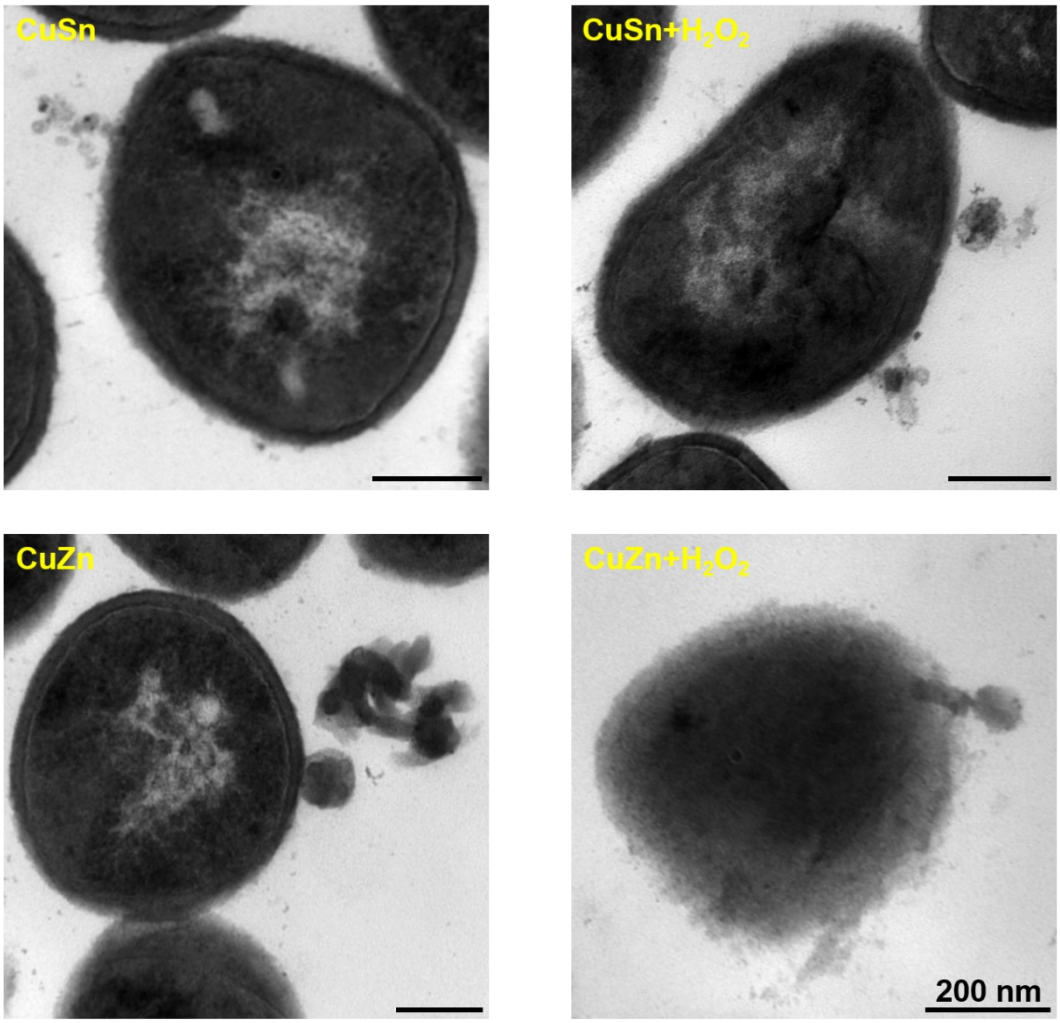

Fig. S13 TEM of *MRSA* treated with different treatments *in vitro*.

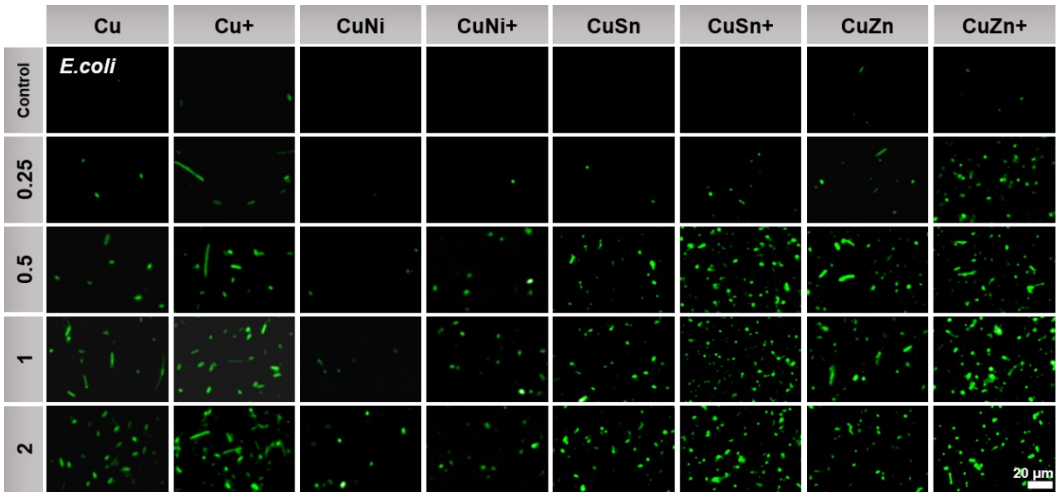

Fig. S14 Fluorescence staining images of *E. coli* using DCFH-DA probe after various treatments.

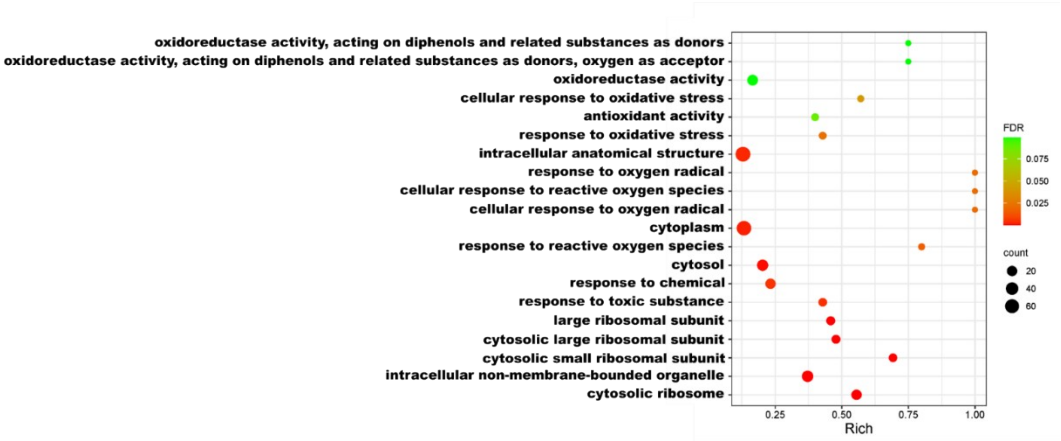

Figure. S15 Rich distribution point diagram of DEGs.

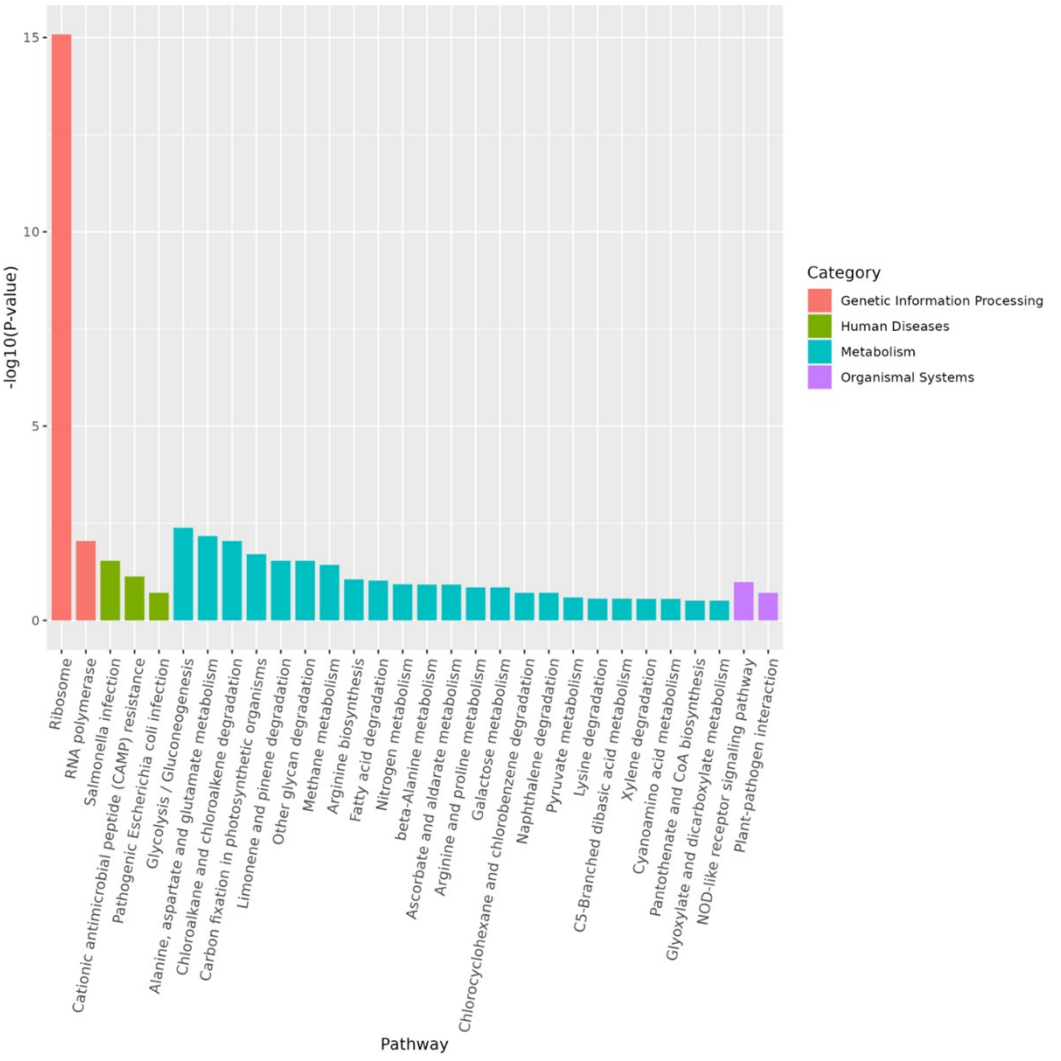

Fig. S16 KEGG analysis of DEGs.

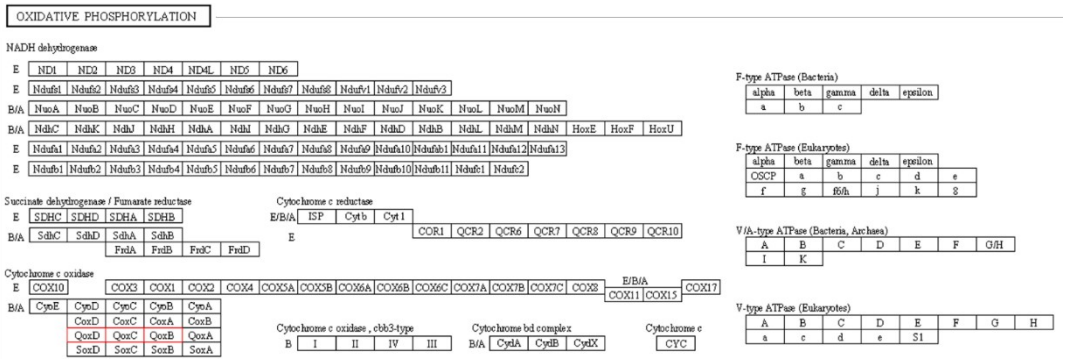

Fig. S17 Schematic diagram of the metabolic pathway (KO-pathway) of oxidative phosphorylation.

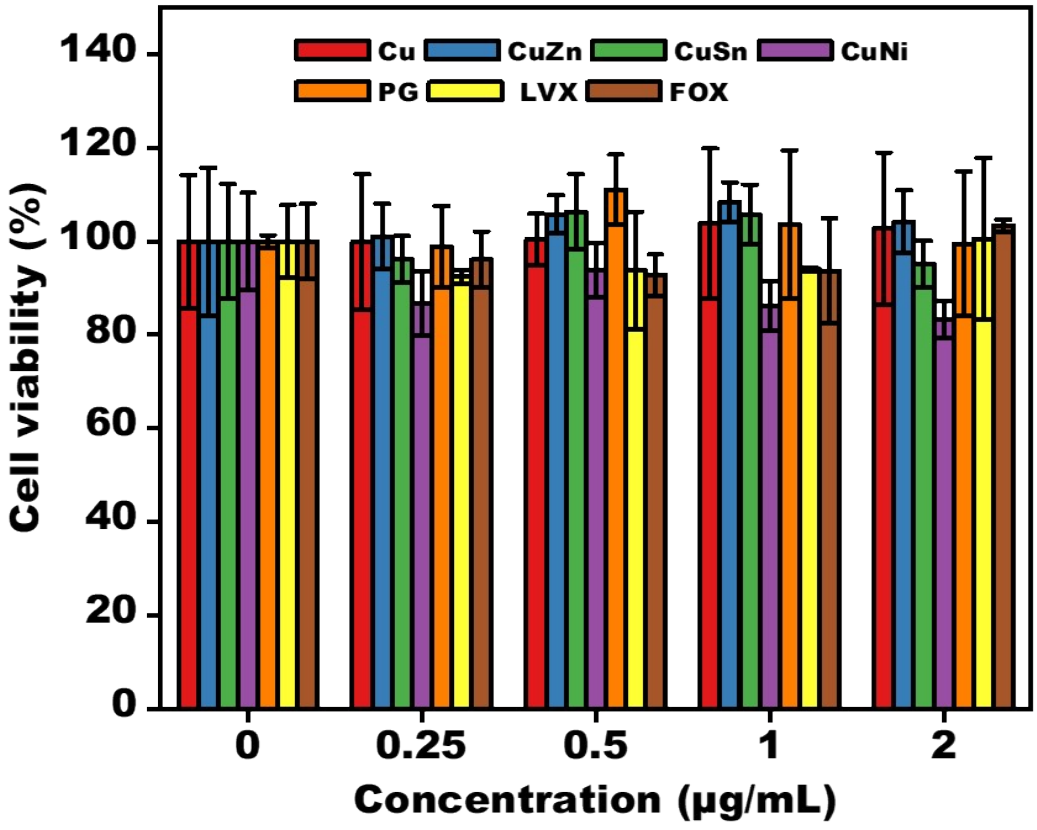

Fig. S18 MTT of HUVECs with different treatments *in vitro*.

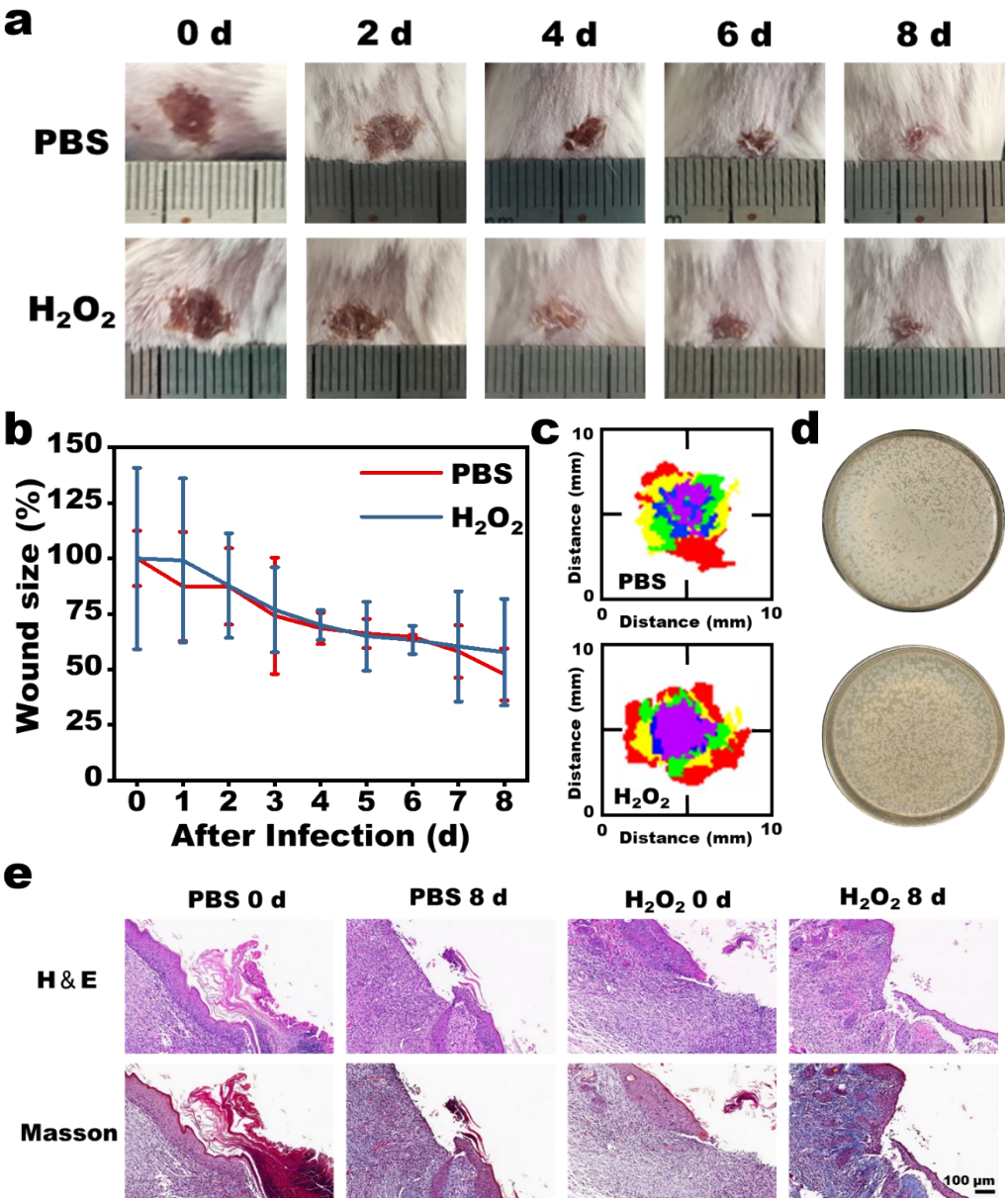

Fig. S19 (a) Therapeutic effects of *MRSA*-infected BALB/c mice after different treatments. (b) Relative wound size (n = 3). (c) wound size radar images at different times. (d) *MRSA* on LB agar grew from the infected wound tissue at the end of different treatments. (e) H&E and Masson staining of the infected tissues.

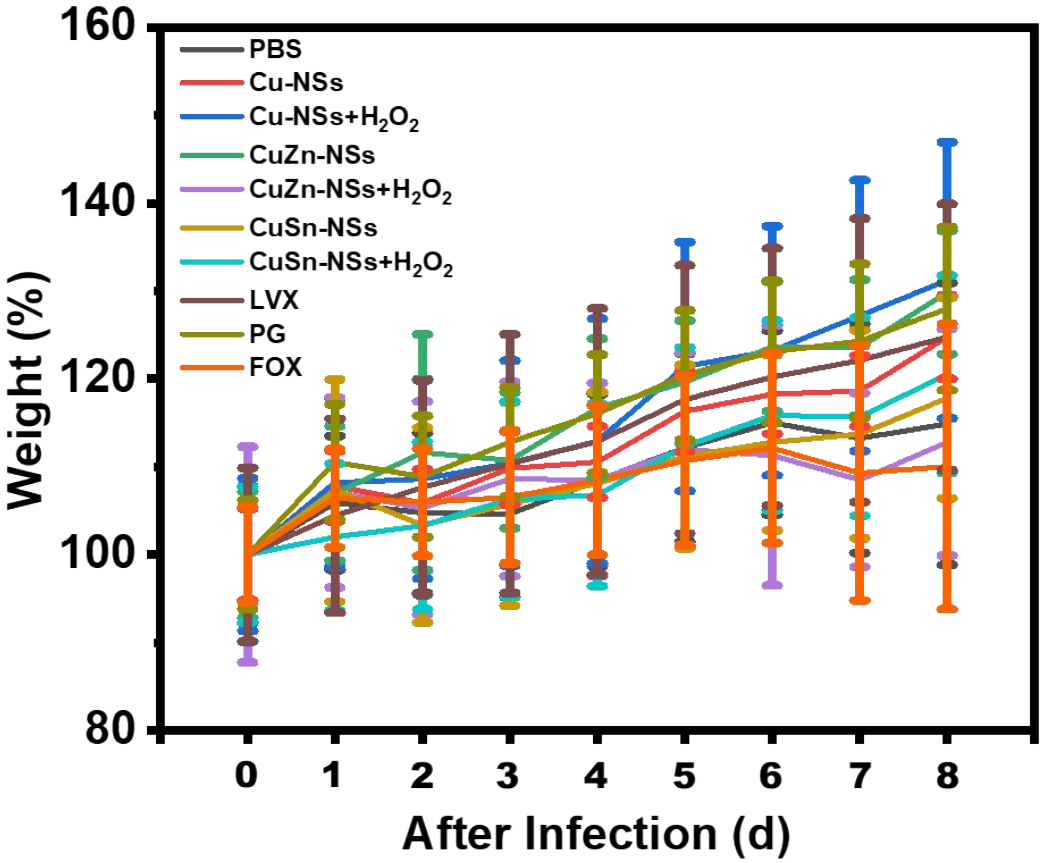

Fig. S20 Body weight of infected mice with different treatments.

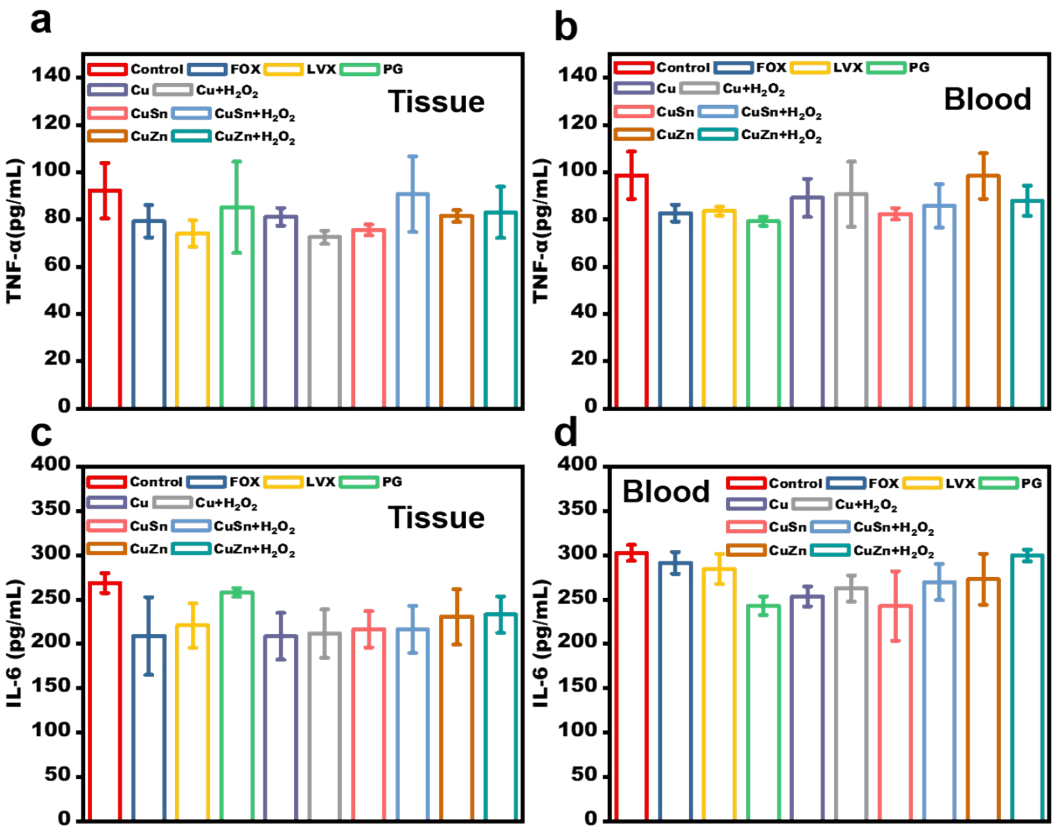

Fig. S21 TNF-α and IL-6 inflammatory factors levels of bacterially infected tissues after different treatments. (a) TNF-α inflammatory factors levels of Wound tissue homogenization after different treatments. (b) TNF-α inflammatory factors levels of serum after different treatments. (c) IL-6 inflammatory factors levels of Wound tissue homogenization after different treatments. (d) IL-6 inflammatory factors levels of serum after different treatments.

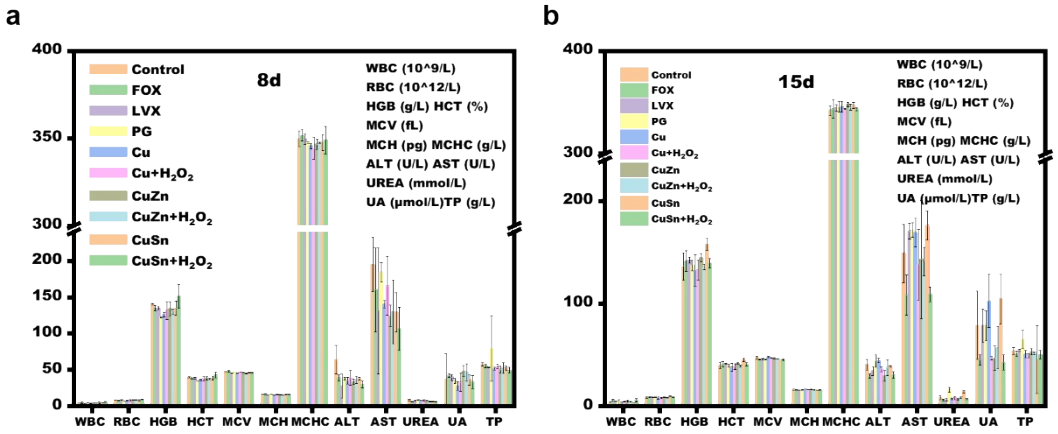

Fig. S22 Blood biochemical analysis of mice after 8 days and 15 days of treatment. (a) Blood biochemical analysis of mice after 8 days of treatment. (b) Blood biochemical analysis of mice after 15 days of treatment.

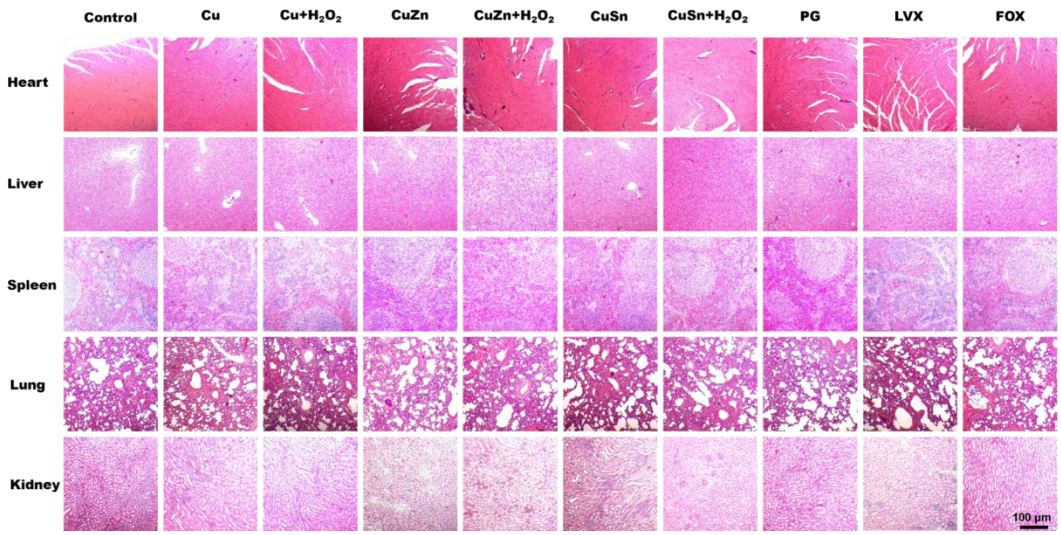

Fig. S23 H&E staining images of major organs after different treatments.

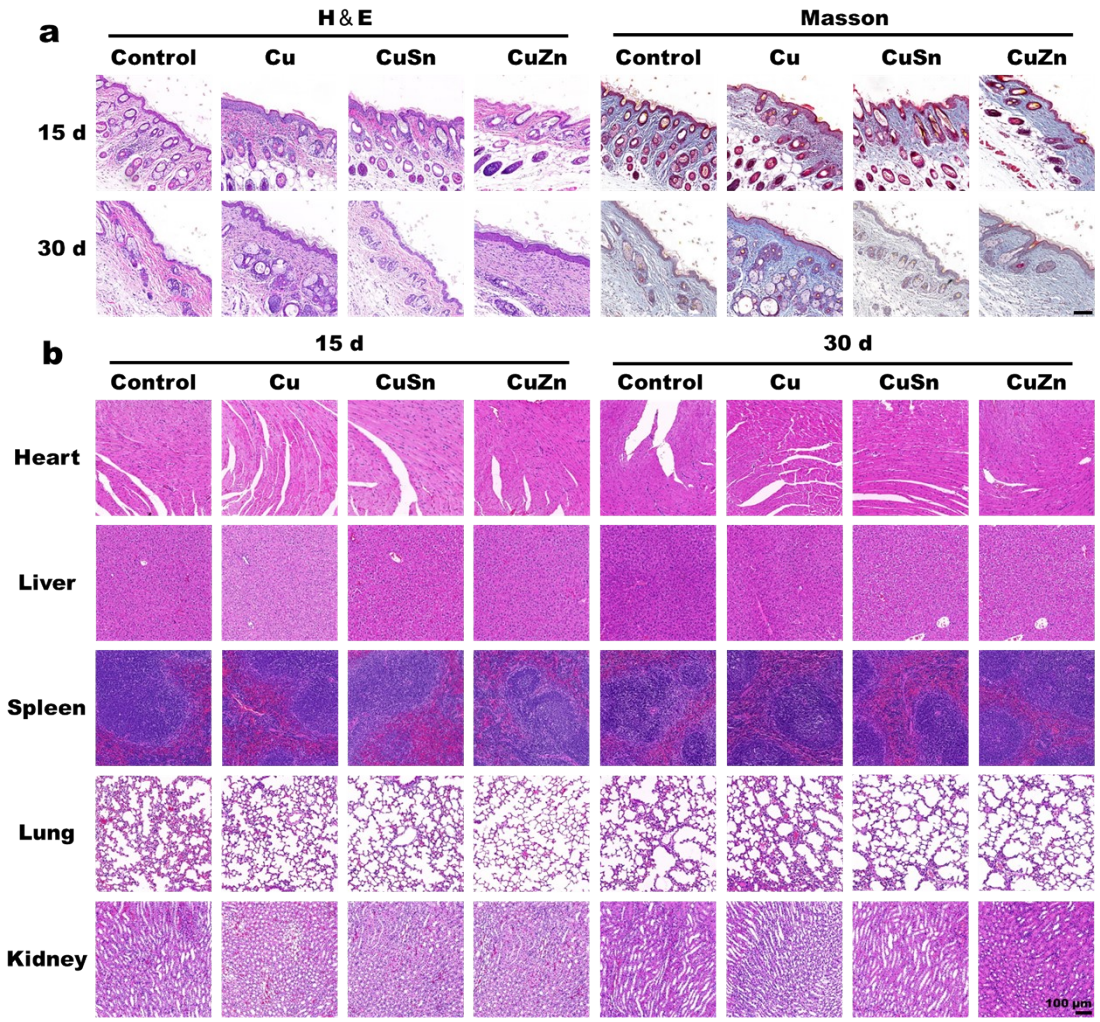

Fig. S24 (a) H&E and Masson staining of the normal tissues. (b) H&E staining images of major organs after different treatments.